

ARISTOTLE UNIVERSITY OF THESSALONIKI

SLAM for Autonomous Planetary Exploration using Global Map Matching

Author:

Dimitrios GEROMICHALOS

Supervisor:

Assoc. Prof. Loukas PETROU

*A thesis submitted to the Faculty of Engineering in
partial fulfillment of the requirements for the degree of*

Diploma
in
Electrical and Computer Engineering

Thessaloniki,
February 2018

Abstract

Write abstract here...

Contents

Abstract	iii
Contents	v
List of Figures	vii
List of Tables	ix
List of Abbreviations	xiii
1 Introduction	1
1.1 Motivation	1
1.2 Problem Statement	1
1.2.1 Presumptions	1
1.3 Literature Review	2
1.3.1 SLAM	2
1.3.2 Planetary Absolute Localization	2
1.4 Thesis Objectives and Outline	2
1.4.1 Research Objectives	2
1.4.2 Outline	3
2 Globally Adaptive SLAM	5
2.1 System Overview	5
2.2 Data Registration	6
2.2.1 Point Cloud Preprocessing	7
2.2.2 Registration	9
Structure of Elevation Map	9
Map Prediction and Update	10
2.3 Data Fusion	11
2.3.1 Sensor Fusion	12
2.4 Pose Estimation	12
2.4.1 Initialization	13
2.4.2 Prediction	14
2.4.3 Update	15
2.4.4 Resampling	16
2.4.5 Estimation	16

2.5	Pose Correction	17
2.5.1	Global to Local Map Matching	18
2.5.2	Criteria Checking	21
	Traversed Distance Criterion	21
	Environment Structure Criterion	22
3	Implementation and Tools	23
3.1	Planetary Rover Testbed	23
3.2	Overall System Architecture	24
3.3	Library	25
3.3.1	Robotic Software Framework	25
3.3.2	Orbiter Data Preprocessing	26
4	Experimental Validation	29
4.1	Scope of Experiments	29
4.1.1	Data Collection	29
4.1.2	Metrics	30
4.2	Experiments on Pose Estimation	31
4.2.1	Relative Localization Results	31
4.3	Experiments on Global Map Matching	34
4.3.1	Absolute Localization Results	34
4.3.2	Map Resolution Viability	36
5	Conclusion	39
5.1	Thesis Summary	39
5.2	Contributions	39
5.3	Directions for Future Extensions	39
5.4	Applications	40

List of Figures

2.1	High level design diagram	6
2.2	Pose estimation activity diagram	14
3.1	Heavy duty planetary rover	23
3.2	System component diagram	25
3.3	ROCK component interface	26
3.4	MARS view from HiRISE	27
4.1	Aerial view of test field	30
4.2	Terrain of first experiment	31
4.3	Traverse of first experiment	32
4.4	Particle filter parameter influence	33
4.5	Terrain of second experiment	34
4.6	Traverse of second experiment	35
4.7	Global gradient map for pose correction	35
4.8	Pose correction error over time plot	36
4.9	Global map resolution comparison	37

List of Tables

4.1	Metrics on parameter sets for relative localization	33
4.2	Results of pose correction for absolute localization	36
4.3	Local and global map resolution viability	38

List of Algorithms

1	Registration of point cloud to map	11
2	Initialization of particle filter	15
3	Estimation of final pose from particle population	17

List of Abbreviations

GA	Globally Adaptive
SLAM	Simultaneous Localization And Mapping
ICP	Iterative Closest Point
KF	Kalman Filter
PF	Particle Filter
PC	Point Cloud
SOR	Statistical Outlier Removal
CV	Computer Vision
TM	Template Matching
SDD	Sum of Square Difference
CCORR	Cross Correlation
CCOEFF	Correlation Coefficient
ROCK	Robot Construction Kit
RTT	Real Time Toolkit
ROS	Robot Operating System
ESA	European Space Agency
NASA	National Aeronautics and Space Administration
HIRISE	High Resolution Imaging Science Experiment
HDPR	Heavy Duty Planetary Rover
GPS	Global Positioning System
TOF	Time Of Flight
LIDAR	Light Detection And Ranging
IMU	Inertial Measurement Unit
SIL	Software In the Loop
MSE	Mean Square Error
RMSD	Root Mean Square Deviation

Chapter 1

Introduction

1.1 Motivation

Mention the scope, its state, the current issues and what is needed to solve them

- Scope: planetary exploration (for scientific purposes)
- State: past and current missions, their purpose and outcome/state
- Issues: no constant communication, manual command sequence, unsafe/upredictable conditions
- Needed: real-time and low-supervision system/platform

1.2 Problem Statement

Mention the environment and the robot's equipment and purpose

Mention that the problem is given X inputs to calculate Y outputs

- Environment: extreme planetary terrains with anomalies (rocks and craters) and high elevation variance
- Equipment: mechanical and sensor configuration
- Purpose: autonomous (low-supervision) navigation
- Inputs: odometry pose, sensor inputs, imu, global map
- Outputs: corrected pose, local elevation map

1.2.1 Presumptions

Explain what presumptions are made to the problem

- Initial global position is known

- Environment is static (not true for autonomous driving applications of algorithm)
- Environment is unknown (no high resolution a priori maps) (not true for autonomous driving applications of algorithm)
- Terrain is single layered (no bridges etc.)

1.3 Literature Review

1.3.1 SLAM

- What is SLAM
 - typical explanation in literature
 - categories
- How is SLAM implemented
 - volumetric/feature based approaches
 - grid-based fast slam
 - etc. etc. etc.

1.3.2 Planetary Absolute Localization

Mention how is absolute localization achieved in planetary applications

- Feature based approaches
- Skyline based approaches
- map based approaches

1.4 Thesis Objectives and Outline

1.4.1 Research Objectives

Mention what are the main objectives in terms of research

- Develop a novel technique for minimizing drift in global localization with global map matching and an execution strategy (criteria)
- Determine under what circumstances (i.e. resolution, local and global) can the orbital imagery be useful for SLAM

- Examine and quantify the gains (better localization, by providing a navigable map with the resolution and dense distribution restrictions that come with it) and loses (processing overhead)

1.4.2 Outline

Explain how this thesis is structured

Chapter 2

Globally Adaptive SLAM

2.1 System Overview

In order for planetary robots to navigate autonomously in extreme and uncertain conditions where no GPS information is available, they need to perceive their surroundings with high precision and maintain this precision over time. A way of compensating for the lack of real-time GPS data, is to use an *a priori* global map that contains 3D information about the environment the robot is trying to navigate into. This map can be reconstructed using imagery taken from an orbiter and has a notably lower resolution compared to the robot's sensory data. To take advantage of this existing information, we have developed a system called *Globally Adaptive SLAM* (*GA SLAM*), which is based around two layers of data processing.

In the first tier, the objective is to perceive the environment and capture its 3D structure so as to enable the robot to navigate in it. This is achieved by constructing a local map and estimating the robot's current pose (position and orientation) w.r.t. its initial pose, using sensory inputs and odometry data. This process is commonly known as *Simultaneous Localization And Mapping* (SLAM) and can be expressed as

$$p(x_{0:T}, m_{1:T} | z_{1:T}, u_{1:T}) \quad (2.1)$$

where x are the estimated poses of the robot, m is the constructed map of the environment, z are the sensory inputs and u are the robot's controls. To reduce the problem's dimensions, the following factorization is performed

$$p(x_{0:T}, m_{1:T} | z_{1:T}, u_{1:T}) = p(x_{0:T} | m_{1:T-1}, z_{1:T}, u_{1:T}) p(m_{1:T} | x_{0:T}, z_{1:T}) \quad (2.2)$$

where the former belief represents the pose estimation problem, also called relative localization, and the latter belief represents the mapping problem.

In the second tier, the objective is to achieve absolute localization by eliminating the accumulated drift which occurs in the previous stage. This drift is present in long-range scenarios and comes from the fact that all the input information is coming

directly from the robot itself. To eliminate it, a matching technique is utilized with the aim of finding the position of the robot's local map inside a global map.

The separation of the system to two layers comes from the need to process the data in separate moments, depending on the conditions of the environment as well as on the robot's processing capabilities. In Figure 2.1, the high-level design diagram of the system shows the 4 main modules that comprise the entire system. Their functionality is explained in the following sections of this chapter.

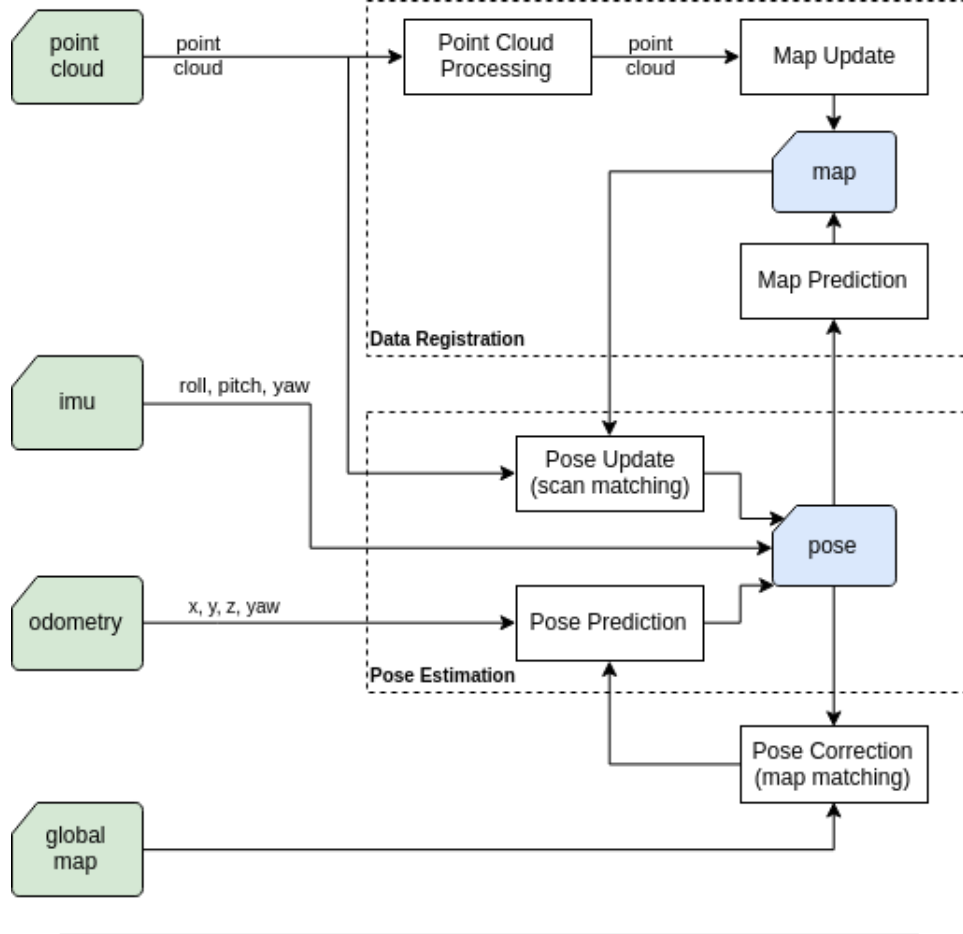


FIGURE 2.1: The high-level design diagram of the GA SLAM system.

2.2 Data Registration

An integral aspect of a robotic system, is the mapping process. In the previous chapter (Section 2.1) this process was expressed as

$$p(m_{1:T} | x_{0:T}, z_{1:T}) \quad (2.3)$$

where m is the posterior map of the environment, x are the estimated poses of the robot and z are the sensory inputs. The map is the model of the environment and can represent information about it in either two or three dimensions. In addition, the

information a map represents can be organized either in a grid-based manner (volumetric map) or in the form of landmarks (feature-based map). Volumetric maps provide a more detailed and precise model of the environment compared to feature-based maps and are, therefore, the better choice for robots that aim to solve navigation tasks. Moreover, autonomous robots that need to navigate in non-flat surfaces, require a 3D model as a means to safely avoid the terrain's obstacles. Robotic applications with this requirement include outdoor, underwater, airborne or planetary missions.

As we have already mentioned, planetary rovers have an important constraint in on-board computational power. This limitation deems the use of pure 3D maps inappropriate. To overcome this problem, we can represent the environment with a 2.5D map, known as elevation map. An elevation map is essentially a 2D grid-map composed of cells that hold the value of the terrain's elevation. It is important to note that this mapping method does not model completely the 3D environment, but can provide a sufficient approximation even for the most demanding applications.

To make use of this mapping technique, a robot must be equipped with a sensor that is capable of providing measurements in the 3D space. Such measurements are usually stored in a structure called point cloud - a set of points P that contain information about their position in space (x, y, z). A point cloud can be constructed from sensors that provide depth information, with the most popular being stereo cameras, time-of-flight (ToF) cameras and LiDARs.

In this section, the functionality of the Data Registration module will be explained. Its main purpose is to preprocess the input sensor data (point cloud) and register it to create an elevation map or update an existing one.

2.2.1 Point Cloud Preprocessing

The importance of preprocessing a point cloud before registering its data in a map, comes from the fact that point clouds contain large amount of points and hence process them is a time-consuming task. Additionally, the points represented in the cloud may be referenced in a different frame (usually the sensor's frame) than the frame of the map.

For this purpose, we implemented a point cloud preprocessing submodule, that consists of the following four steps:

1. **Voxelization:** In this step, we reduce the volume of the point cloud by down-sampling it using a discrete 3D grid. Each cell of the grid, called *voxel*, is mapped to $\{0, 1\}$ and it therefore represents the existence or absence of an obstacle in that position. This method is called *voxelization* and results in a more sparse cloud of 3D points.

2. **Transformation:** A point P sampled from the sensor is in the sensor's reference frame S and need to be transformed in the map's frame M in order to be registered. This is achieved by

$$\mathbf{t}_{MP} = \mathbf{R}_{SM}\mathbf{t}_{SP} - \mathbf{t}_{SM} \quad (2.4)$$

where \mathbf{t}_{MP} is the position of P in the map frame, \mathbf{t}_{SP} is the position of P in the sensor frame, \mathbf{R}_{SM} is the rotation between the sensor frame and the map frame and \mathbf{t}_{SM} is the translation between them.

3. **Cropping:** Since a point cloud can span a wide area in space depending on the sensor's field of view and orientation, we can further reduce the volume of the cloud by discarding (cropping) points that fall out of the map. This is done by defining a box in space and removing from the point set all the points that are not inside it. In our case, we define the minimum and maximum cutoff points that represent the diagonal of the crop box as

$$\begin{aligned} min_cutoff_point &= \left(-\frac{l_x}{2} - t_x, -\frac{l_y}{2} - t_y, z_{min} \right) \\ max_cutoff_point &= \left(\frac{l_x}{2} + t_x, \frac{l_y}{2} + t_y, z_{max} \right) \end{aligned} \quad (2.5)$$

where l_x and l_y are the lengths of the map in meters in the x and y axis, t_x and t_y are the positions of the map in meters in the x and y axis and z_{min} and z_{max} are the minimum and maximum elevation of the map.

4. **Uncertainty calculation:** In this last step, we use the sensor's model to calculate the variance of each point in the point cloud, σ_z^2 . As a result, each point will contain in addition to a x and y position, a one-dimensional Gaussian distribution $\{z, \sigma_z^2\}$ for the height. The z value is calculated by applying the projection matrix $\mathbf{P} = [0 \ 0 \ 1]$ to the transformed point using the Equation 2.4:

$$z = \mathbf{P}(\mathbf{R}_{SM}\mathbf{t}_{SP} - \mathbf{t}_{SM}) \quad (2.6)$$

This equation can also be written as

$$z = f(\mathbf{t}_{SP}) \quad (2.7)$$

where $f : \mathbb{R}^3 \rightarrow \mathbb{R}$ is a non linear function.

To obtain the variance value of the transformed point, we propagate the uncertainty of the initial point as

$$\sigma_z^2 = \Sigma^f = \mathbf{J} \Sigma^{\mathbf{t}_{SP}} \mathbf{J}^\top \quad (2.8)$$

where Σ^f is the variance-covariance matrix of f , $\Sigma^{t_{SP}}$ is the covariance matrix of the initial point and \mathbf{J} is the Jacobian matrix of f defined as

$$\mathbf{J} = \frac{\partial f}{\partial t_{SP}} = \mathbf{P} \mathbf{R}_{SM} \quad (2.9)$$

The covariance matrix for a point in the point cloud is defined as

$$\Sigma^{t_{SP}} = \begin{bmatrix} \sigma_{xx}^2 & \sigma_{xy}^2 & \sigma_{xz}^2 \\ \sigma_{yx}^2 & \sigma_{yy}^2 & \sigma_{yz}^2 \\ \sigma_{zx}^2 & \sigma_{zy}^2 & \sigma_{zz}^2 \end{bmatrix} \quad (2.10)$$

and is different for every sensor, since it depends on the sensor's model and characteristics. For example, for a stereo camera we approximate the variance of the point in three dimensions with a quadratic equation:

$$\sigma^2 = \frac{c \cdot \tan(0.5 \cdot f)}{0.5 \cdot b \cdot w} d^2 \quad (2.11)$$

where c is the search range or disparity precision, f is the field of view, b is the baseline, w is the horizontal resolution of the camera and d is the range of the point.

2.2.2 Registration

Structure of Elevation Map

The elevation map, also referred to as *local map* or simply *map*, is a robot-centric grid-based map. This means that it is centered in the robot's position in the global reference frame. When the robot moves, previous cells that now fall out of the map are reset and values that belong to the new explored area take their place.

The map models the elevation of the environment as well as the uncertainty of it. As a result, in every position of the 2D grid, the elevation is represented by a one-dimensional Gaussian distribution. This means that the map consists of two layers

- the layer of *mean* elevation (μ_z) and
- the layer of elevation *variance* (σ_z^2)

Apart from its structure, a map is also characterized by a few other properties. The most important are

- the *resolution*, which is the dimension of a cell in meters,
- the *length*, which is the length of the map in meters,
- the *minimum* and *maximum* elevation values that the map can hold,

- the 2D *position* of the map in the global reference frame and
- the *orientation* of the map in the global reference frame

Regarding the last property, it is worth mentioning that the orientation of the map is fixed w.r.t. to the global frame. This decision was made with a focus on reducing the complexity when performing a prediction of the map (see next section).

Map Prediction and Update

Even though the map prediction and update steps are grouped in the same submodule, they implement two separate functionalities. The map prediction is triggered when a new odometry pose is received and processed by the Pose Estimation module (Section 2.4). The map update is triggered as soon as a new point cloud arrives from the sensor.

• Prediction

This step is responsible for moving the map when the robot assumes a new position. This is essentially a simple 2D transformation of the map's position in the x and y axes. The robot's orientation is not taken into account, since as we said earlier (Section 2.2.2), the orientation of the map about the z axis is fixed. To perform the prediction, we simply

1. apply the delta translation (t_x, t_y) of the new estimated pose to map and
2. keep the height Gaussian $\mathcal{N}(\mu_z, \sigma_z^2)$ of each cell unchanged

When a translation is applied to the map, cells that fall out of the map have their values reset and elevation values of the new explored area take their place instead. To avoid unnecessary data copying in memory, the data storage can be implemented as a two-dimensional circular buffer.

• Update

This is the core step of the Data Registration module, since this step implements the registration of the input point cloud into the map. The algorithm of the point cloud projection is shown in Algorithm 1.

It uses a probabilistic approach to take advantage of the fact that both the point cloud (Section 2.2.1) and the map (Section 2.2.2) represent the elevation as a one-dimensional Gaussian distribution. The last operation of the algorithm (Operation 22) is the actual fusion, and can be implemented with different methods. A popular method is the one used in a Kalman filter, which given two Gaussian distributions $\mathcal{N}(\mu_1, \sigma_1^2)$ and $\mathcal{N}(\mu_2, \sigma_2^2)$, can be implemented as

$$\text{innovation} = \mu_2 - \mu_1 \quad (2.12)$$

$$gain = \frac{\sigma_1^2}{\sigma_1^2 + \sigma_2^2} \quad (2.13)$$

$$\mu_1 = \mu_1 + gain \cdot innovation \quad (2.14)$$

$$\sigma_1^2 = (1 - gain) \cdot \sigma_1^2 \quad (2.15)$$

Algorithm 1 Registration of point cloud to map

```

1:  $M_\mu$ : mean elevation layer of the map
2:  $M_{\sigma^2}$ : variance elevation layer of the map
3:  $P$ : point cloud - set of  $\{x, y, z\}$ 
4:  $V$ : point cloud variances - set of  $\{\sigma_z^2\}$ 
5:
6: for each  $p$  in the  $P$  do ▷ iterate through all points
7:   if position of  $p$  is outside of map then
8:     continue
9:
10:   $\mu_{point} \leftarrow p[z]$  ▷ projection of the point
11:   $\sigma_{point}^2 \leftarrow V[p]$ 
12:
13:   $index \leftarrow find\_map\_index(p[x], p[y])$  ▷ corresponding cell in grid
14:
15:   $\mu_{cell} \leftarrow M_\mu[index]$ 
16:   $\sigma_{cell}^2 \leftarrow M_{\sigma^2}[index]$ 
17:
18:  if  $\mu_{cell}$  or  $\sigma_{cell}^2$  is not initialized then
19:     $\mu_{cell} \leftarrow \mu_{point}$ 
20:     $\sigma_{cell}^2 \leftarrow \sigma_{point}^2$ 
21:  else
22:     $\mathcal{N}(\mu_{cell}, \sigma_{cell}^2) \leftarrow \mathcal{N}(\mu_{cell}, \sigma_{cell}^2) \cdot \mathcal{N}(\mu_{point}, \sigma_{point}^2)$ 
23:
24:   $M_\mu[index] \leftarrow \mu_{cell}$ 
25:   $M_{\sigma^2}[index] \leftarrow \sigma_{cell}^2$ 
  
```

2.3 Data Fusion

The goal of this module is to fuse data from different sources and increase the overall quality of the map. This is achieved by taking advantage the already computed uncertainty estimates in the map and applying fusion techniques to improve the existing data. In particular, we developed two submodules to perform fusion in separate stages of the pipeline. These are explained in the following sections.

2.3.1 Sensor Fusion

Using sensor fusion we can exploit the multiple sensors equipped in a robot to increase the covered area in the map. In addition to increased coverage, fusing sensor data that are overlapping in the map can increase its quality.

The way a point cloud is registered (fused) in the map, was already mentioned in a previous section (Section 2.2.2). Using this method we can combine information from different sensors, as long as the input data is in the form of a point cloud, by simply updating the map and taking advantage of the uncertainty estimates that are calculated in the preprocessing of the point cloud.

A drawback of this technique is that large calibration errors and inaccuracies in the transformations (\mathbf{t}_{SM} and \mathbf{R}_{SM}) between a sensor and the map can have the opposite effect i.e. deteriorate the map quality. This is due to the fact that fusion can over-smooth obstacles since their correspondence in the map will be slightly different for each sensor. Errors like these can easily produce false negative obstacles and have a detrimental effect in the navigation of the robot.

2.4 Pose Estimation

The pose, or state, of a robot navigating in a 3D environment, consists of its position (x, y, z) and its orientation ($roll, pitch, yaw$) w.r.t. a global reference frame. Hence, the goal of pose estimation, also referred to as relative localization, is to accurately track the robot's pose in the environment. This is usually accomplished by either employing a probabilistic filter, e.g. a Kalman filter or a particle filter, or by utilizing methods such as scan matching. A filter's inputs are usually expressed in the form of position or velocity and can be extracted using odometry techniques. In comparison, the input of a scan matching method is by definition a scan, i.e. measurement, received by a sensor. For our case, we approached the localization problem by making use of a combination of scan matching and particle filtering techniques.

First, we assume the state of the problem to be

$$\mathbf{x} = [x \ y \ z \ roll \ pitch \ yaw]^\top \quad (2.16)$$

where $roll$, $pitch$ and yaw are the rotations about the x , y and z axes respectively. However, we cannot obtain accurate estimates for the $roll$ and $pitch$ states from odometry. To overcome this limitation, we use an *inertial measurement unit* (IMU) sensor and receive these states directly from it, so the problem state becomes

$$\mathbf{x} = [x \ y \ z \ yaw]^\top \quad (2.17)$$

By making the assumption that the z estimation from odometry is accurate in an area near the robot, the state can be further simplified as

$$\mathbf{x} = [x \ y \ yaw]^\top \quad (2.18)$$

which is also referred to as

$$\mathbf{x} = [x \ y \ \theta]^\top \quad (2.19)$$

In the case where this assumption is false, the result will be a deformed map, since the elevation values of the map will be directly affected by the wrong z estimate of the robot.

We employ a particle filter that samples particles in a continuous state space to estimate the posterior of the robot's state

$$p(x_{0:T} \mid m_{1:T-1}, z_{1:T}, u_{1:T}) \quad (2.20)$$

where m is the constructed map of the environment, z are the sensory inputs and u are the odometry inputs. This is done by using the odometry inputs to predict the state of each particle and the sensory inputs, i.e. point clouds, for the weight update. Additionally, the uncertainty of each particle is modeled using a Gaussian distribution. Finally, yaw measurements from the robot's IMU sensor are fused with the final estimate to provide more accurate measurements.

An activity diagram illustrating the algorithm's steps is shown in Figure 2.2. These steps are explained in detail in the following sections.

2.4.1 Initialization

This step is executed only during the initialization of the algorithm, or when the particle filter is reset and the objective is to sample each particle using a Gaussian distribution. The probability density function of the distribution $\mathcal{N}(\mu, \sigma^2)$ is

$$f(x \mid \mu, \sigma^2) = \frac{1}{\sqrt{2\pi\sigma^2}} e^{-\frac{(x-\mu)^2}{2\sigma^2}} \quad (2.21)$$

where μ is the mean of the distribution, σ is the standard deviation and σ^2 is the variance. Using this function, the state of each particle is sampled, as shown in Algorithm 2.

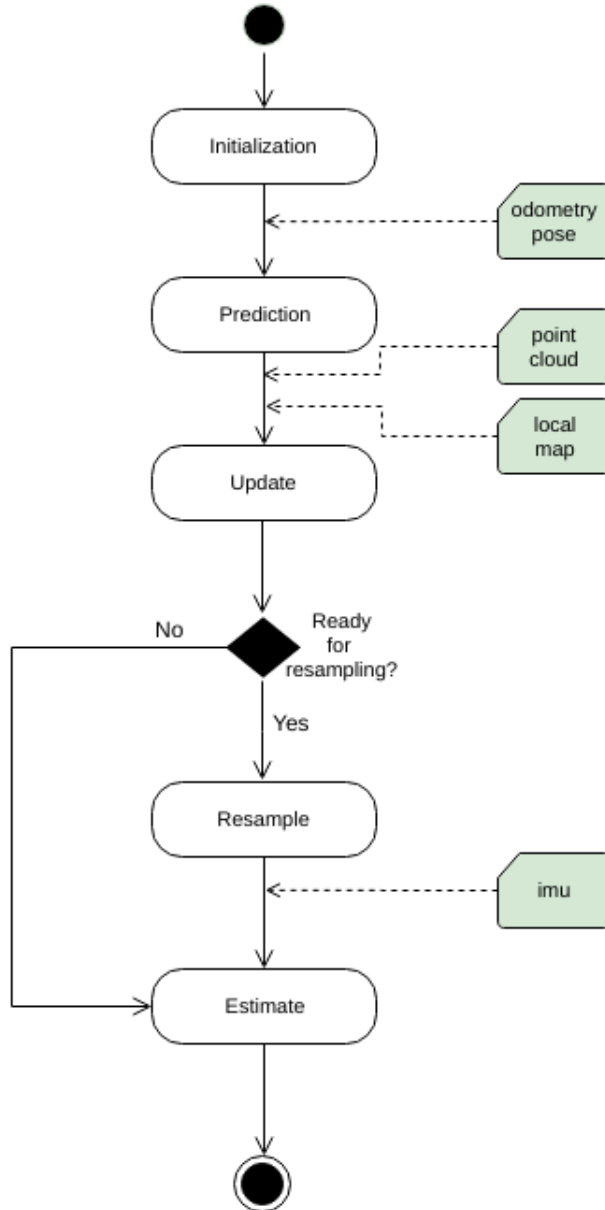


FIGURE 2.2: Activity diagram of the pose estimation module.

2.4.2 Prediction

When a new odometry input u_t is received, the state of each particle p_i is sampled using the prediction as the mean value of a Gaussian distribution as such

$$x_t^i \sim \mathcal{N}(x_{t-1}^i + \Delta x_t, \sigma_x^2) \quad (2.22)$$

$$y_t^i \sim \mathcal{N}(y_{t-1}^i + \Delta y_t, \sigma_y^2) \quad (2.23)$$

$$\theta_t^i \sim \mathcal{N}(\theta_{t-1}^i + \Delta \theta_t, \sigma_\theta^2) \quad (2.24)$$

Algorithm 2 Initialization of particle filter

```

1:  $P$ : set of particles with  $\{\{x, y, \theta\}, weight\}$ 
2:
3: for each  $p$  in the  $P$  do
4:    $x \sim \mathcal{N}(\mu_x, \sigma_x^2)$                                  $\triangleright$  sample the states from their distributions
5:    $y \sim \mathcal{N}(\mu_y, \sigma_y^2)$ 
6:    $\theta \sim \mathcal{N}(\mu_\theta, \sigma_\theta^2)$ 

```

where x_i , y_i and θ_i represent the state of the particle, Δx , Δy and $\Delta \theta$ are the delta inputs from odometry and σ_x^2 , σ_y^2 and σ_θ^2 are the variances of the states that define the Gaussian noise that will be added to the particle.

2.4.3 Update

When a new point cloud measurement z_t is received, the weight of each particle p_i is updated using scan matching. In particular, for every particle, the input point cloud is matched with a point cloud extracted from the robot's local map using an Iterative Closest Point (ICP) variant.

For the purpose of achieving a fast convergence of the ICP, we first preprocess the inputs as such: (i) crop the raw point cloud (sensor scan) to the local map's size (ii) convert local map to a point cloud using the elevation values of the grid map (iii) downsample both point clouds using a voxel grid (in a similar way as in Section 2.2.1).

In addition, the point cloud extracted from the local map is transformed to each particle's state (pose) and as a result each particle holds a representation of the environment according to its hypothesis. Since the weight of each particle is proportional to the uncertainty of its hypothesis, it can be updated by measuring the degree of alignment between the raw point cloud and the particle's point cloud.

One way to measure the alignment between a source point cloud $S = \{s_1, s_2, \dots, s_{N_s}\}$ and a reference point cloud $R = \{r_1, r_2, \dots, r_{N_r}\}$ is by computing the sum of the squared error

$$e = \frac{1}{N_r} \sum_{i=1}^{N_r} \|s_i - r_i\|^2 \quad (2.25)$$

where s_i and r_i are the points which correspond to each other.

An easy method of performing this computation is to run one iteration of the ICP algorithm and using the output fitness score as the point cloud alignment error. Therefore, the weight w_i of a particle p_i is calculated as

$$w_i = \frac{1}{icp_fitness_score} \quad (2.26)$$

2.4.4 Resampling

The act of resampling the set of particles of the filter is done to ensure that the particle population models the uncertainty of the problem as close as possible. Although there are several variants that can be exploited to solve the resampling problem depending on the situation, we make use of a fairly common technique called multinomial resampling.

Given a particle set of N particles, a cumulative distribution is initially formed by normalizing the weight of each particle as

$$w_i = \frac{w_i}{\sum_{k=0}^N w_k} \quad (2.27)$$

where w_i is the weight of a particle p_i from the particle set. From the cumulative distribution, N new particles are sampled uniformly while maintaining the state of each particle.

It is obvious that particles which were associated with a high weight in the previous population have a higher chance of being selected. Thus, a new population is created that possibly contains duplicate particles. These particles will be scattered again in the next iteration by adding Gaussian noise in the prediction step (Section 2.4.2).

An important aspect of resampling is the resampling strategy used, i.e. the moment that resampling is performed in the population. Depending on the parameters of the particle filter as well as on the states of the problem, different strategies yield different results. In our approach, we adopted a simple strategy that resamples every K iterations of the algorithm. This parameter depends on the robot's controls as well as on the magnitude of the Gaussian noise added to each particle and can be configured accordingly for each application.

2.4.5 Estimation

The last step of the algorithm is to extract the final pose estimate from the particle filter. This is accomplished in two steps: (i) estimate pose from the particle cloud (ii) fuse pose with measurements from an IMU sensor.

In many applications of the particle filter, the first step is achieved by simply picking the best particle, i.e. the particle with the highest weight in the particle set. However, using this method, when the best particle is removed from the population during resampling, choosing the next best particle will cause the robot to "teleport" in the continuous space, hence deforming the constructed map. To overcome this issue, we have implemented a technique (Algorithm 3) that extracts the pose by thresholding particles with low weight and averaging the remaining.

Algorithm 3 Estimation of final pose from particle population

```

1:  $P$ : set of particles
2:  $p$ : particle - set of  $\{states, weight\}$ 
3:
4:  $S \leftarrow \{\}$                                       $\triangleright$  candidate particles
5: for each  $p$  in  $P$  do
6:   if  $p[w] > w_{threshold}$  then                 $\triangleright$  remove uncertain particles
7:      $S \leftarrow S + p$ 
8:
9: Sort  $S$  by weight
10:  $M \leftarrow S[1 : k]$                                  $\triangleright$  pick top  $k$  particles
11:
12:  $w_{sum} \leftarrow \sum_{i=1}^k w_i$ 
13:  $x \leftarrow \sum_{i=1}^k w_i x_i / w_{sum}$             $\triangleright$  weighted average of each state
14:  $y \leftarrow \sum_{i=1}^k w_i y_i / w_{sum}$ 
15:  $\theta \leftarrow \sum_{i=1}^k w_i \theta_i / w_{sum}$ 

```

Finally, to further improve the estimation, we fuse the *yaw* measurement from the IMU sensor with the *yaw* estimate from the particle filter. The fusion is done by means of one-dimensional Gaussian distributions, hence we need to associate a variance to each value.

The IMU Gaussian is represented as $\mathcal{N}(\mu_{imu}, \sigma_{imu}^2)$ where μ_{imu} is the measurement value from the sensor and σ_{imu}^2 is the variance which is a parameter that represents how reliable the sensor is. The second Gaussian is represented as $\mathcal{N}(\mu_\theta, \sigma_\theta^2)$, where μ_θ is the *yaw* estimate that was extracted in the previous step and σ_θ^2 is the variance of the distribution. It can be calculated by applying the formula for a weighted standard deviation as

$$\sigma_\theta = \sqrt{\frac{\sum_{i=1}^N w_i (\theta_i - \mu_\theta)^2}{\sum_{i=1}^N w_i}} \quad (2.28)$$

where N is the number of particles, w_i is the weight of each particle and θ_i is the *yaw* hypothesis of each particle. The fusion of the two distributions is performed in a similar fashion as in the Data Registration module (Section 2.2.2).

2.5 Pose Correction

Although the robot's pose is constantly tracked using a particle filter in the Pose Estimation module (Section 2.4), the approach is still based on dead-reckoning due to the fact that all the inputs of the process arrive from internal sensors. As a result, a localization error is accumulated in long-range traverses and the robot's pose in the global reference frame is unknown. With the aim of bounding this error and achieve

absolute (global) localization, we have developed an extra component in the system that eliminates the drift by matching the local map to an *a priori* global one.

The global map can be reconstructed using imagery taken from an orbiter (satellite), although its resolution cannot reach the level of the local one. Furthermore, in contrast to the local map which is always centered around the robot, the global map is referenced in the global frame, i.e. the same coordinate system as the robot's pose. This enables us to match the two maps and apply the delta transformation to correct the drifted pose.

2.5.1 Global to Local Map Matching

The matching of 2D images (frames) is a topic that has been extensively researched in the field of computer vision and several techniques have been developed for that purpose. Since grid-based 2D maps are essentially images, it is possible to apply these techniques to maps as well. The act of matching two images consists of either finding the absolute position of the first image inside the second one or finding a certain correspondence between the two.

Popular approaches vary from simple and statistical-based ones such as comparing the histogram of the images to find similarities, to more complex and efficient ones such as template matching and feature matching. The former, template matching, is a method that convolves a search image (template) with the one being searched into (source) and is usually used to find a smaller image in a bigger one. The latter, feature matching, is based on the idea of extracting a feature set from each image and comparing the two sets in order to find correspondences among them.

Although feature matching is usually the most efficient method, it can yield sub-optimal results in scenarios where features are almost indistinguishable and their extraction contains uncertainties. For this reason, we chose to base our matching approach on a template matching method and exploit the feature-sparse environment of our planetary application.

The proposed algorithm consists of the following three steps:

- **Preprocessing**

Template matching requires the two images to be of the same resolution. Since, as we mentioned earlier, the global image (source image) has a lower resolution than the local image (template image), it is necessary to downsample the local one to match the resolution of the global. To achieve this, we scale the template image with the local to global resolution ratio using a nearest-neighbor interpolation method.

As we discussed in the implementation of the Pose Estimation component (Section 2.4), the long-term drift of the z estimation which is received directly

from odometry, causes an elevation offset in the local map. To overcome this offset, it is possible to match the gradients (first derivatives) of the two images instead of directly matching the normal ones, by applying the Sobel operator in the two images.

The computation of the gradient of an image I , requires first the computation of the gradients in the x and y axes by convolving I with a Sobel odd-sized kernel. For a kernel size of three, the kernel in the horizontal direction is

$$K_x = \begin{bmatrix} -1 & 0 & +1 \\ -2 & 0 & +2 \\ -1 & 0 & +1 \end{bmatrix} \quad (2.29)$$

and in the vertical direction is

$$K_y = \begin{bmatrix} -1 & -2 & -1 \\ 0 & 0 & 0 \\ +1 & +2 & +1 \end{bmatrix} \quad (2.30)$$

Thus, the two gradients are computed as

$$G_x = K_x * I \quad (2.31)$$

$$G_y = K_y * I \quad (2.32)$$

and the final magnitude of the gradient is calculated by combining both gradients:

$$G = \sqrt{G_x^2 + G_y^2} \quad (2.33)$$

Finally, we replace unknown cell values, i.e. cells that do not contain an elevation value, with zero since the matching method we use cannot handle unknown values. It is also possible to mask these values during matching. In any case, zero values do not contribute to the outcome of the match as it is explained in the next step.

• Matching

A drawback of template matching compared to feature matching is that it cannot match rotated images, and therefore it cannot find a yaw correction in the robot's global pose. To overcome this limitation, we warp (rotate) the template image in a discrete angle space, e.g. from -10° to 10° with a step of 1° . As a result, we run template matching for every individual angle (e.g. twenty times for the previous example) and choose the yaw correction angle that provides the best result.

Template matching works by sliding the template image T pixel-by-pixel in the source image I and comparing at each location the two images using a metric

(score). Then for each location of T over I , the score is stored in a result matrix R . Consequently, the location in R where the score is highest, is the location of the best match.

The metric used to compare the images, greatly influences the final result. The most popular metrics used are:

1. the Sum of Square Difference (SDD), which is expressed as

$$R(x, y) = \sum_{x', y'} (T(x', y') - I(x + x', y + y'))^2 \quad (2.34)$$

where x' and y' correspond to the pixel (location) of a specific pass.

2. the Cross Correlation, which is expressed as

$$R(x, y) = \sum_{x', y'} (T(x', y') \cdot I(x + x', y + y')) \quad (2.35)$$

3. the Correlation Coefficient, which is expressed as

$$R(x, y) = \sum_{x', y'} (T'(x', y') \cdot I'(x + x', y + y')) \quad (2.36)$$

where

$$T'(x', y') = T(x', y') - \frac{\sum_{x'', y''} T(x'', y'')}{width \cdot height} \quad (2.37)$$

$$I'(x + x', y + y') = I(x + x', y + y') - \frac{\sum_{x'', y''} I(x + x'', y + y'')}{width \cdot height} \quad (2.38)$$

Since, the invalid cells of the template image have been converted to zero, the last method cannot be used because these cells would affect the result. After experimental evaluation of the first and the second metrics, we came to the conclusion that the second method (Equation 2.35) yields more optimal results for our application.

In addition, it is practical to normalize the metric to produce a metric that scales with the size and intensity of the template and source images. The new metric becomes:

$$R(x, y) = \frac{\sum_{x', y'} (T(x', y') \cdot I(x + x', y + y'))}{\sqrt{\sum_{x', y'} T(x', y')^2 \cdot \sum_{x', y'} I(x + x', y + y')^2}} \quad (2.39)$$

Another advantage of the normalization of the metric, is that it provides an output score in the fixed range $[0 \dots 1]$, with 1 being a perfect match. Using that, we can provide certain guarantees to the matching by selecting the best match only when the score is above a specific threshold (e.g. 95%).

- **Correction**

The last step consists of converting the position (x, y) of the match from image coordinates to map coordinates:

$$x_{map} = \left\lfloor \frac{h}{2} \right\rfloor - x_{image} \quad (2.40)$$

$$y_{map} = \left\lfloor \frac{w}{2} \right\rfloor - y_{image} \quad (2.41)$$

where h and w are the height and width of the template image respectively.

Finally, we apply the correction (x, y, θ) to the particle filter as a control input, i.e. all the particles are updated using this delta transformation. Doing that, we ensure that Gaussian noise will be added to each particle, as specified in Section 2.4.2.

2.5.2 Criteria Checking

Absolute map-based localization techniques are known to be time consuming, since they require the processing of a large amount of data. In our case, template matching works by comparing the local map to a patch of the global map for every pixel of the latter. Furthermore, this process is executed multiple times for a discrete space of angles values with the aim to correct the drift in *yaw* in addition to the 2D position correction. It becomes obvious that a proper execution strategy has to be adopted so as to avoid the use of unnecessary processing power.

For planetary applications, since energy efficiency is of utmost importance, it is common for rovers to focus only on one task at each moment. Thus, an absolute localization task cannot be run in the middle of a traverse, where the robot's motors are at full power. An approach that takes this limitation into consideration, is to execute the task in the end of the day, when the rover recharges and only secondary tasks are scheduled.

Nevertheless, as energy-efficient task scheduling is out of the scope of this work, we have proposed a practical solution that can be utilized alongside the rest of the system. For this purpose, two criteria are defined that have to be checked before a global to local map matching is initiated. The first criterion defines the minimum distance the robot must cover and the second criterion defines the structure of the environment that the pose correction module works in.

Traversed Distance Criterion

To minimize the execution overhead of the map matching process, it would be sensible to correct the localization's accumulated drift only when it surpasses a certain

level. For this purpose, we defined a threshold distance value that the robot must traverse before a new correction can take place:

$$\sqrt{(x - x_0)^2 + (y - y_0)^2} > d_{threshold} \quad (2.42)$$

where $\{x, y\}$ is the current position of the robot, $\{x_0, y_0\}$ is the position of the last pose correction and $d_{threshold}$ is the traversed distance threshold value. It is important to notice that the robot's traversed distance is calculated in two dimensions, since the correction is also expressed in terms of $\{x, y\}$.

By taking into account the fact that the delta pose that results from the map matching process is in the same order of magnitude as the global map's scale, the threshold value should be proportional to it as well. In addition, the threshold depends on the accuracy of the pose estimation as well as on the speed of the robot, and should be chosen accordingly for each application.

Environment Structure Criterion

With the exception of localization techniques that rely on global navigation satellite systems (e.g. GPS), the existence of some form of surrounding features is necessary for a robot to localize itself. As a result, we defined a second criterion that takes into account the structure of the environment by checking for elevation features.

This is achieved in four steps: (i) create a gradient image from the local elevation map by calculating the gradient in elevation (similarly to the map matching preprocessing step of Section 2.5.1) (ii) threshold the gradient image to remove low gradient values (iii) add remaining values to get total gradient value (iv) compare total value to threshold.

The threshold compared to the total gradient value is a parameter that mainly depends on the morphological characteristics of the terrain. Furthermore, it should be tuned according to the resolution of the local map since the sum of the map's gradients is proportional to the map's scale.

Chapter 3

Implementation and Tools

3.1 Planetary Rover Testbed

In order to benchmark our system in real scenarios, we implemented the system in a testbed rover and integrated it with the rest of its components. The rover we used is named Heavy Duty Planetary Rover (HDPR) and is capable of traversing different types of terrain with a speed of up to 1 m/sec. It was developed by the Automation and Robotics Lab (ARL/TEC-MMA) of the European Space Agency (ESA) and is currently used for validating software and hardware components in long range scenarios.

The HDPR rover, depicted in Figure 3.1, bears close resemblance to the camera setup of the ExoMars mission rover and allows the evaluation of algorithms that have a focus on autonomous navigation. Specifically, the sensor suite of the rover comprises of the following components:



FIGURE 3.1: The Heavy duty planetary rover (HDPR).

- Exteroceptive:
 - LocCam stereo camera (PointGrey Bumblebee 2)
 - PanCam stereo camera (PointGrey Grasshopper 2)
 - Kinect time of flight camera
 - MESA SR4500 time of flight camera
 - Velodyne LiDAR (VLP-16)
- Proprioceptive:
 - Trimble GNSS receiver (BD970)
 - Inertial Measurement Unit (Sensonor STIM300)
 - Shaft Encoders and Potentiometers

From these sensors, we exploit (i) the LocCam for visual odometry inputs and (ii) the PanCam for SLAM inputs. The LocCam has a baseline of 120 mm, is positioned about 1.1 m above the ground and is tilted at an angle of 18°. The PanCam has a baseline of 500 mm, is positioned about 1.9 m above the ground, is tilted at an angle of 19° and has a field of view (FoV) of 40°.

In addition, the Inertial Measurement Unit (IMU) provides measurements about the orientation and acceleration of the robot. Although the rest of the sensors are not actively used by our system, they can be exploited for validation purposes.

3.2 Overall System Architecture

As we mentioned previously, the GA SLAM system was designed to function with point cloud based inputs in addition to odometry inputs.

To utilize the sensor suite of the HDPR rover, we can extract point clouds using stereo processing techniques and odometry estimation using visual odometry methods. For the former we employ the PanCam stereo camera and for the latter we make use of the LocCam stereo camera. Furthermore, we exploit the measurements received from the IMU to augment the estimation of the robot's pose. The utilization of each sensor of the HDPR rover w.r.t. to our system, is shown in the system component diagram of Figure 3.2.

As depicted, the local elevation map of the GA SLAM subsystem can be used in order to extract a map that contains traversability features about the surrounding environment of the rover, i.e. features that determine if the rover is able to traverse a specific area. At a next layer, the traversability map and the estimated pose from SLAM can be utilized by a path planning module, with the aim to provide autonomously control the rover in an unknown environment. Finally, It should be

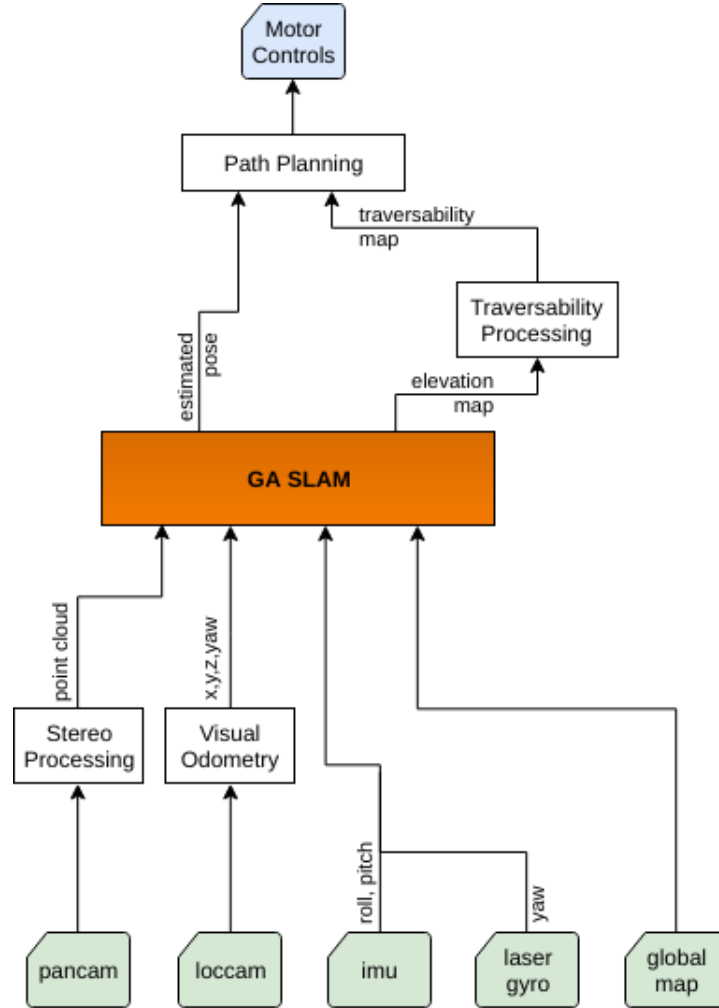


FIGURE 3.2: The components of the system that enable the HDPR to perform autonomous navigation tasks.

noted that the choice of visual odometry instead of plain wheel odometry, comes from the fact that a robot is prone to slippage in outdoor environments, and more specifically planetary terrains.

3.3 Library

3.3.1 Robotic Software Framework

The GA SLAM system was implemented as a framework-independent library for C++ and depends only on libraries for linear algebra, point cloud processing and image processing. However, with the aim to provide integration with the rest of HDPR's software modules and tools, we developed a component to bridge the library using the Robot Construction Toolkit (ROCK).

ROCK is a software framework for the development of robotic systems, similar to Robot Operating System (ROS). It differs from ROS in the sense that the development of applications is achieved using a model driven approach. It is implemented on top of the Orococos Real-Time Toolkit (Orococos RTT) component layer and can provide real-time capabilities to a system. In addition, it contains a rich collection of reliable and extensible modules that are ready to use as well as tools for visualization and task monitoring.

In ROCK, each distinct functionality of the system is encapsulated in an RTT component (Figure 3.3) using a tool called *oroGen*. This tool, auto-generates the C++ code of the component, given the specification of the component's interface. The communication with the rest of the ROCK universe, is implemented through a network of connected components. This is achieved using the framework's Ruby modules which support the explicit interconnection of a component's input port(s) with the output port(s) of another component.

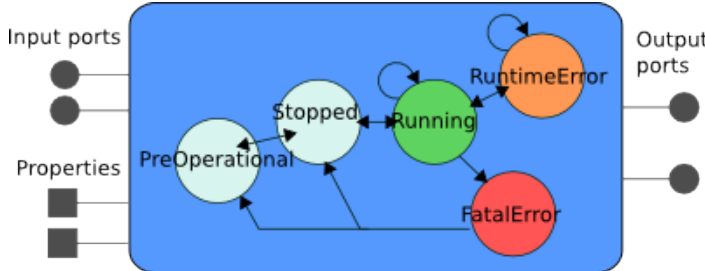


FIGURE 3.3: The interface and the state machine of a component in the Orococos Real-Time Toolkit. The output port(s) of a component can be explicitly connected to the input port(s) of another component. The properties are used to configure the component internally.

3.3.2 Orbiter Data Preprocessing

As a means to validate the map matching capabilities of the system, an orbiter (global) map is necessary. A real example of such map has beeен reconstructed using orbital imagery, depicted in Figure 3.4, that was captured using the High Resolution Imaging Science Experiment (HiRISE) camera mounted on NASA's Mars Reconnaissance Orbiter (MRO).

It is possible to emulate an orbiter map using drone imagery. The aerial images can then be used to reconstruct and provide a 3D representation of the captured scene in the form of a densified point cloud. At a later stage, the constructed point cloud can be projected in a 2D grid and create an elevation map.

Prior to the projection, it is necessary to preprocess the global point cloud in order to simplify it and transform it to a known reference system. This is achieved in 4 steps: (i) voxelize point cloud to the desired resolution (ii) crop the voxel grid in the order

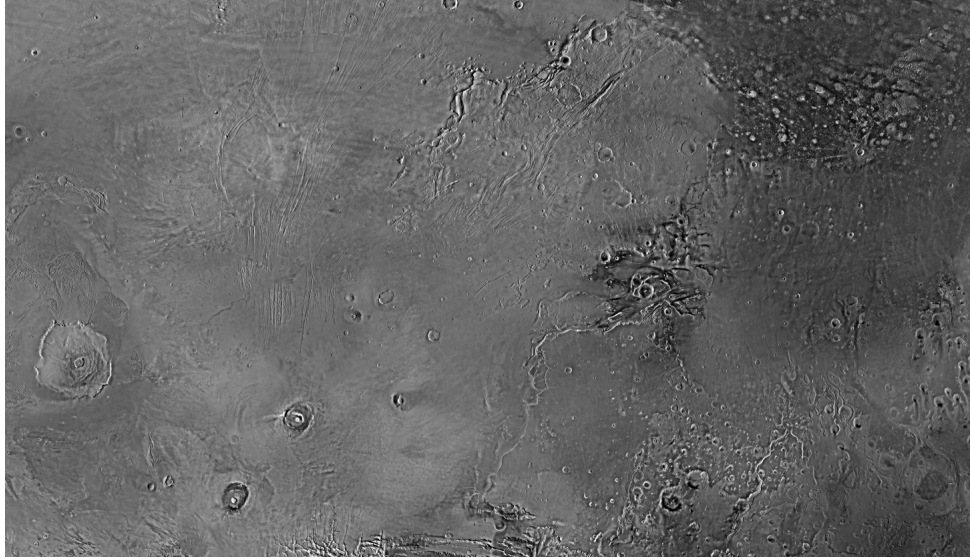


FIGURE 3.4: Close view of MARS that was captured using the HiRISE camera mounted on the Mars Reconnaissance Orbiter.

of magnitude as the local map's size instead of using the whole information (e.g. for a local map of $10\text{ m} \times 10\text{ m}$ crop the grid to $100\text{ m} \times 100\text{ m}$) (iii) smooth the voxel grid using a Statistical Outlier Removal (SOR) filter which rejects points that are far from their neighbors (iv) transform the voxel grid to the robot's initial absolute pose.

Chapter 4

Experimental Validation

4.1 Scope of Experiments

The purpose of the experiments is to validate the proposed system as well as its robustness in various terrains and configurations. Since the autonomous navigation of the robot is out of the scope of this thesis, the mapping procedure is only indirectly validated as part of the SLAM system. Thus, the main focus of the experiments is the relative and absolute localization techniques that were developed.

4.1.1 Data Collection

The performed experiments were executed by means of *Software In the Loop* (SIL) tests using precollected data. The data were collected by the Planetary Robotics Lab team of the European Space Agency as part of a two week test campaign that took place in the Minas de San Jose desert in Tenerife, Spain with the aim to validate the integration of the HDPR rover (Section 3.1) and provide data for future research projects. The aerial view of the local is presented in Figure 4.1.

For that reason, the collected dataset contains samples from: (i) three stereo camera sensors (ii) IMU sensor (iii) point clouds reconstructed from drone imagery (iv) GPS sensor. These samples are used both as input to our system and as ground truth information.

The environment in which the test data were collected, was chosen with the aim to bear close resemblance to rough planetary terrains, specifically to the one of Mars. In particular, various geological properties such as the distribution and the shape of the rocks is similar to the Martian terrain.

Finally, the speed of the robot in these datasets was chosen to be close to the 10 cm/sec value, considering the long-range traverses it was required to cover. As such, for the first two experiments, the size of the local map is fixed at 20 m × 20 m and its resolution at 10 cm/cell, while for the global map we presumed the resolution to be fixed

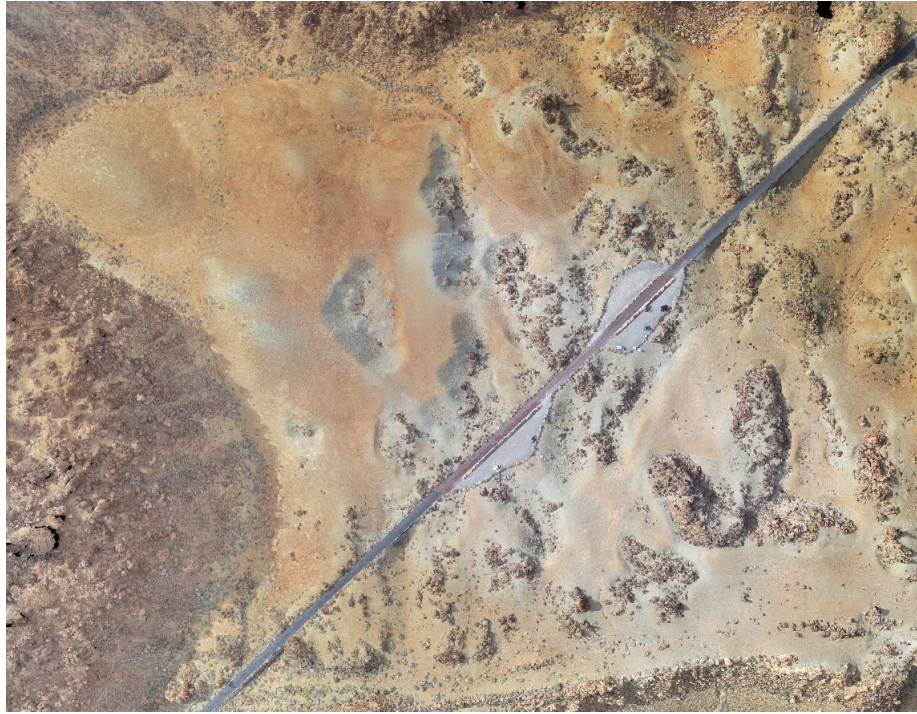


FIGURE 4.1: Aerial view of test field that was reconstructed using drone imagery.

at 50 cm/cell. In the third experiment, the performance of our approach is validated against these parameters, hence they are variable.

4.1.2 Metrics

To quantify the experimental results and evaluate the outputs of the system, it is necessary to introduce certain metrics:

- **Mean square error (MSE) of pose graph:** This is a straightforward metric for benchmarking SLAM algorithms and can be defined as

$$\varepsilon_{MSE}(\hat{x}_{1:T}) = \frac{1}{T} \sum_{t=1}^T (\hat{x}_t \ominus x_t)^2 \quad (4.1)$$

where $\hat{x}_{1:T}$ is the estimated pose graph, $x_{1:T}$ is the ground truth pose graph, T is the number of samples and $x_i \ominus x_j$ is the distance between two poses.

- **Root mean square deviation (RMSD) of pose graph:** Similarly to the MSE metric, this metric expresses the sample standard deviation of the differences between the estimated and the ground truth poses and can be defined as

$$\varepsilon_{RMSD}(\hat{x}_{1:T}) = \sqrt{\frac{1}{T} \sum_{t=1}^T (y_t - \varepsilon_{MSE})^2} \quad (4.2)$$

where y_t is defined as $\hat{x}_t \ominus x_t$.

4.2 Experiments on Pose Estimation

4.2.1 Relative Localization Results

The purpose of this experiment is to test the accuracy of the Pose Estimation module (see Section 2.4) and evaluate its capabilities in a relative localization (short-range) scenario. To accomplish that, we will carry out each experiment with different parameter sets with the aim of examining the system’s sensitivity as well as finding an optimal parameter configuration.

The main parameters that we will tune during the experiments are all related to the particle filter and include (i) the number of particles used (ii) the resampling frequency (iii) the standard deviation of the Gaussian noise added to each particle. Finally, the expected error of the estimated pose should ideally be in the same order of magnitude as the size of one cell of the local map, so as to ensure that the robot can distinguish the environment’s obstacles with a high-level of certainty.

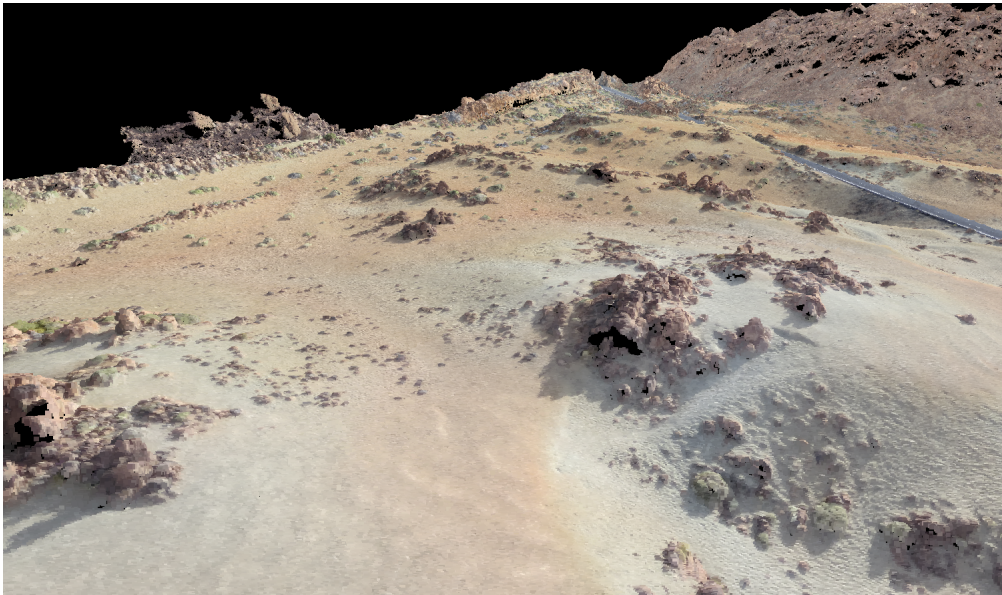


FIGURE 4.2: 3D view of the terrain evaluated in the first experiment.

Figure 4.2 presents a view of the evaluated terrain of the first scenario. The terrain is depicted in the form of one dense point cloud which was reconstructed from drone imagery. The bird’s eye view in Figures 4.3b and 4.3c shows the traverse of the robot in this scenario and compares the ground truth path, the one from raw visual odometry and the one from the pose estimation. In contrast to the visual odometry estimate (blue path), the pose estimate of our system (red path) follows closely the ground truth (black path). The richness of the terrain in features, which is visible in

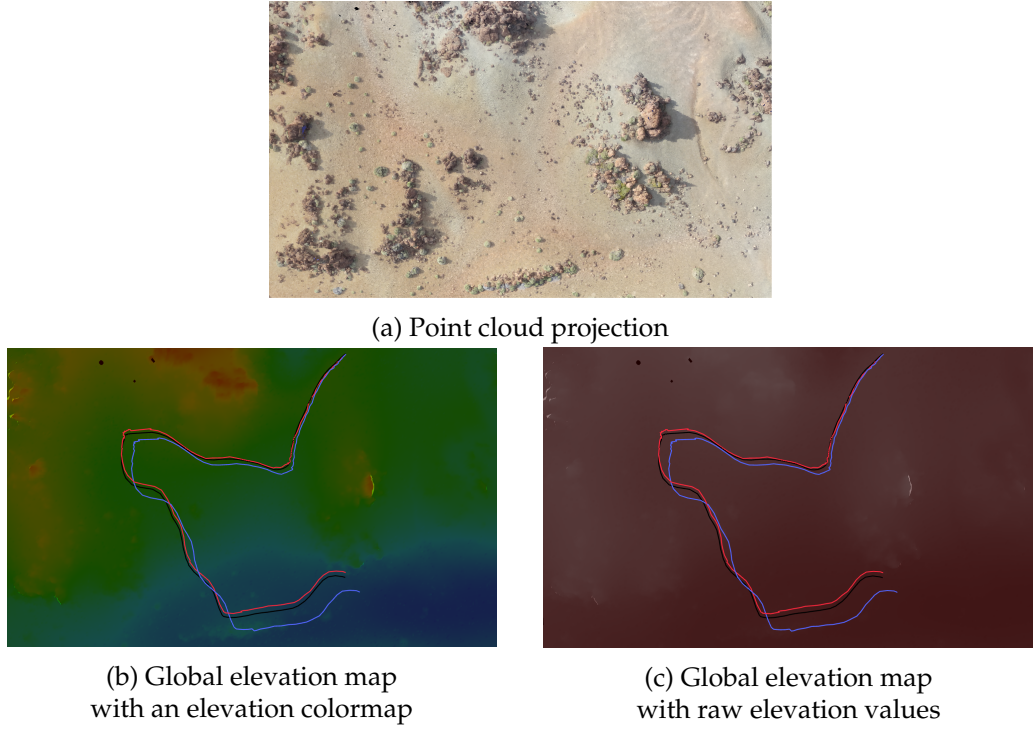


FIGURE 4.3: Orthographic views of the environment and the robot’s traverses in it. The black, red and blue colors correspond to the ground truth, SLAM and visual odometry paths accordingly.

Figure 4.3a, is an advantage for relative localization since the weights of the particles in the particle filter are updated using scan matching.

In particular, the influence the number of particles used has on the outcome is shown in the comparison plot in Figure 4.4a. We observe that the pose error decreases as we increase the number of particles used in the particle filter, since the continuous space of the problem is modelled more effectively. However, increasing this parameter, brings a proportional increase to the computation needs for every iteration of the filter. As it is visible in the plot, a justified choice would be to use 100 particles for a balance of error and processing power. Furthermore, it is important to notice that the drift in pose (20 cm in the case of 100 particles), is proportional to the robot’s speed (10 cm/sec in this experiment).

Regarding the second parameter, the plot in Figure 4.4b represents the same error as the previous plots, with the difference that the number of particles is fixed to the value of 100 and the resampling frequency is the variable parameter. It is visible that resampling too often or too rare has an impact on the pose error. This is due to the fact that by resampling, the particle population is gathered near the best belief and as a result other possible solutions are eliminated.

For the purpose of further quantifying the results of this scenario altogether, we calculate the *MSE* and *RMSD* metrics (defined in Section 4.1.2) for the parameter sets that were used to generate the above plots. The values of these metrics are presented

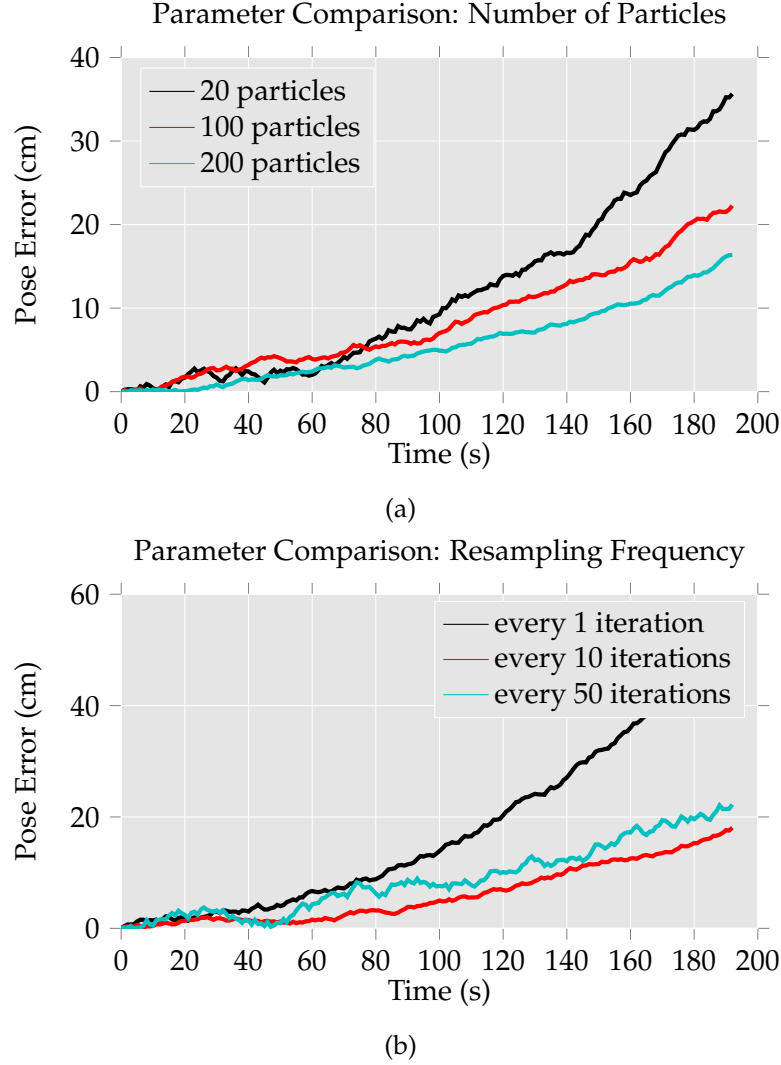


FIGURE 4.4: (a) The influence the number of particles has on the pose error. (b) The influence the resampling frequency parameter has on the error.

in Table 4.1. The conclusion we drew from the plots are further confirmed using the two metrics, since it is visible that the combination of a low number of particles and a very low or very high resampling frequency increases the mean square error and deviation by more than a factor of 4.

Particle Number	Resampling frequency	MSE	RMSD
20	10	301.6	287.3
100	10	61.1	55.7
200	10	46.4	41.3
100	1	252.0	240.8
100	10	61.1	55.7
100	50	168.4	157.5

TABLE 4.1: Values of the *MSE* and *RMSD* metrics on different sets of parameters.

4.3 Experiments on Global Map Matching

4.3.1 Absolute Localization Results

Contrary to relative localization, which is the ability to track the robot's pose, absolute localization is the ability to maintain the tracked pose which diverges due to accumulated errors over time. For this purpose, we will test the system in a long-range scenario where localization drifts are manifested and assess the robustness of the Pose Correction module (see Section 2.5). Similarly to the pose estimation experiments, the expected error of the corrected pose should ideally be in the same order of magnitude as the size of one cell of the global map, in consideration of the fact that the global map's resolution is higher than the resolution of the local map.

In the first scenario we evaluate the pose correction functionality in a terrain with average feature richness, i.e. a terrain that contains an average amount of elevation features such as rocks. Figure 4.5 presents the view of such terrain as a dense point cloud and Figure 4.6 shows the traverse inside it. It is visible that the SLAM estimation (red path) has a notable drift from the ground truth values (black path). Near the end of the traverse, we can observe the correction of the robot's pose due to a successful match of the local to global elevation map.

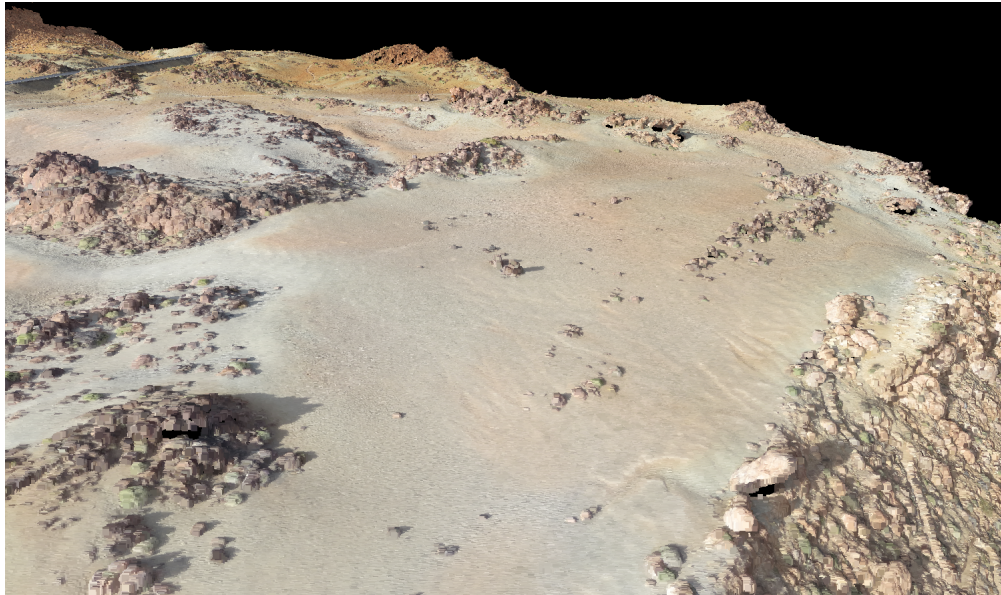


FIGURE 4.5: 3D view of the terrain evaluated in the second experiment.

In addition, we present the orthographic projections of the gradient of the global elevation map (Figure 4.7) where the elevation features are more visible.

The correction of the accumulated error is more visible in the plot of Figure 4.8. The score of the yielded result from the global to local map matching, as well as the rate of correction, are visible in Table 4.2. We can notice that the score of the match is

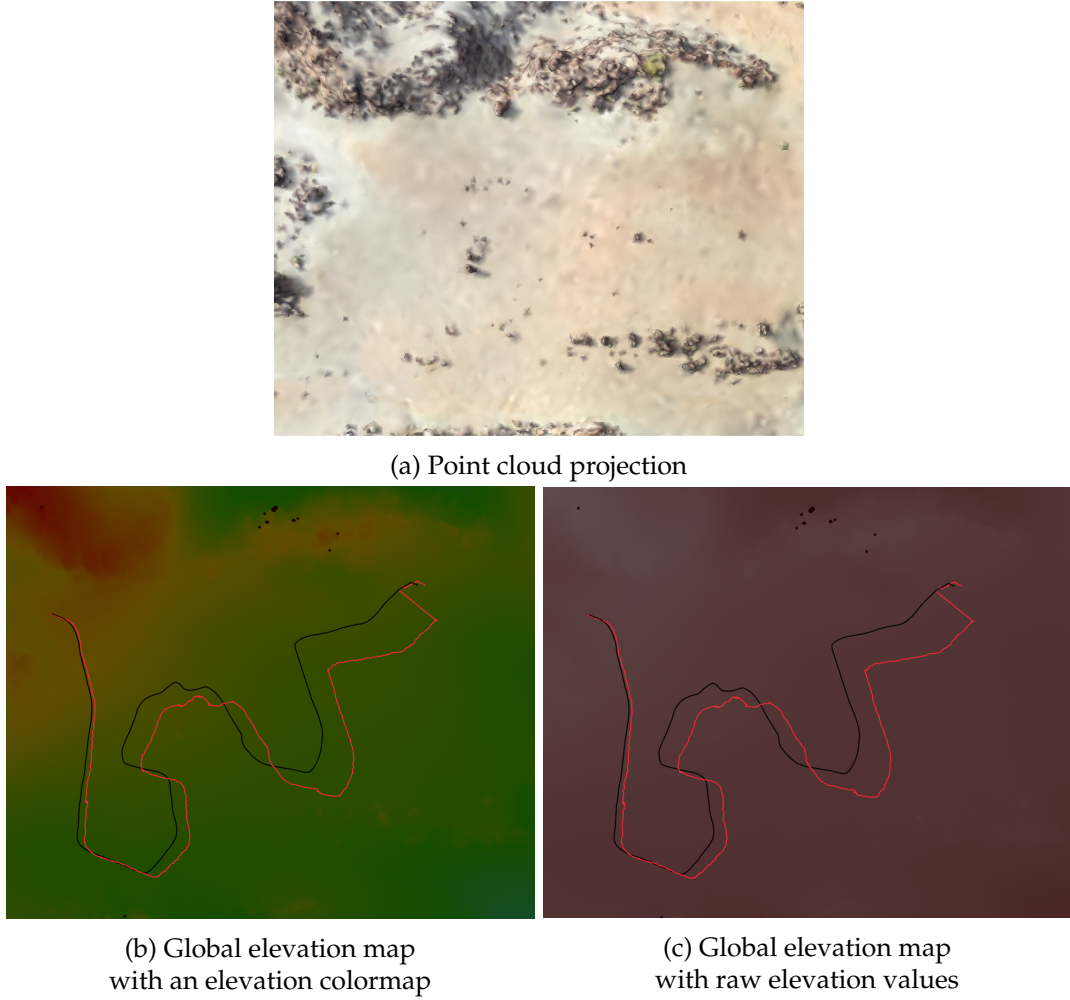


FIGURE 4.6: Orthographic views of the environment and the robot’s traverses in it. The black and red colors correspond to the ground truth and SLAM paths accordingly. The pose correction is visible in the end of the traverse.

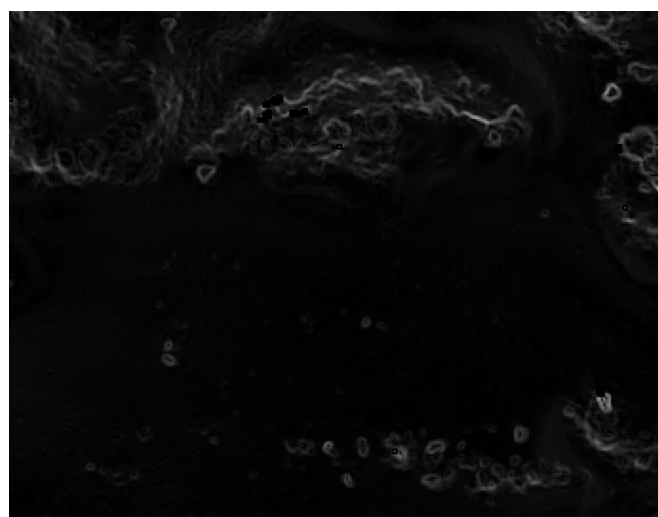


FIGURE 4.7: The global gradient map that the local map is matched to for pose correction.

97.1% (where 100% is a perfect match - as defined in Section 2.5.1) and since the matching threshold was set to 95%, the match is accepted and used to correct the robot's pose by 98.6%.

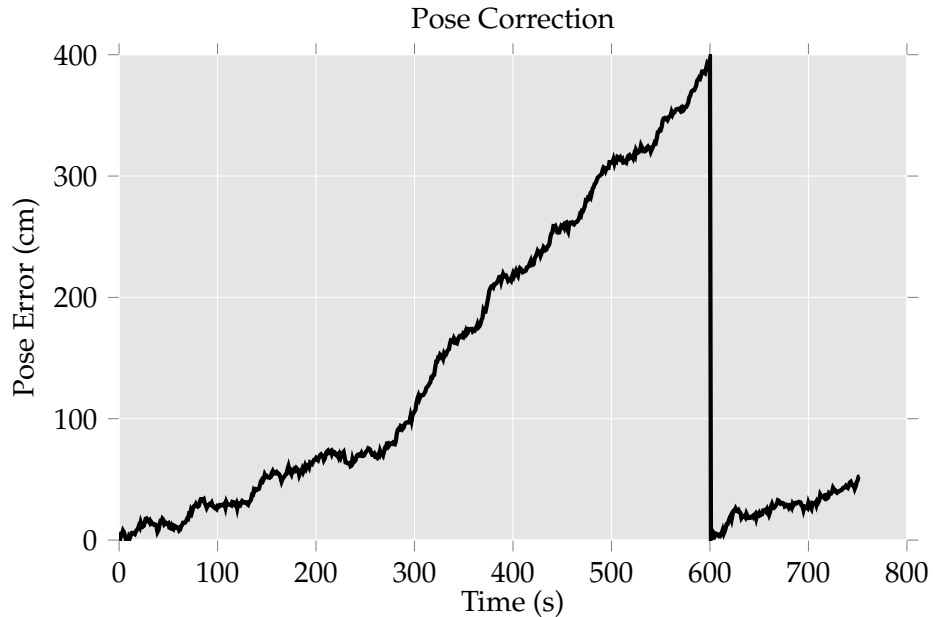


FIGURE 4.8: Pose correction results of second experiment.

Execution time of one iteration	630 ms
Total execution time	12.6 sec
Percentage of correction in position	98.6%
Percentage of correction in orientation	82.9%
Score of the matched location	97.1%
Acceptance threshold of match	95%

TABLE 4.2: Resulting time, correction and score of the match found.

As we already mentioned, the exact moment of correction is determined by the two criteria that were defined in the implementation of the Pose Correction module (see Section 2.5.2). However, since both of them are straightforward, their experimental validation is left out.

4.3.2 Map Resolution Viability

In this experiment, we validate and measure the performance of our map matching technique for absolute localization by performing the same scenarios with different combinations of resolutions for the local and global maps. This is done with the aim to draw conclusions regarding the viability of our approach w.r.t. the available global map data as well as the processing capabilities of a robot.

Figure 4.9 presents the local and global elevation maps with distinct resolution values. Upon matching these maps, we observe the score of each match for every combination of resolutions (Table 4.3). We can notice that a low resolution global map has more impact in the map matching score than a low resolution local map. In fact, a global map with a resolution of 2.0 m/pixel yields poor results for every resolution of the local map. On the other hand, a global map with a resolution of 1.0 m/pixel has the possibility to yield a high score only when the resolution of the local map is high enough.

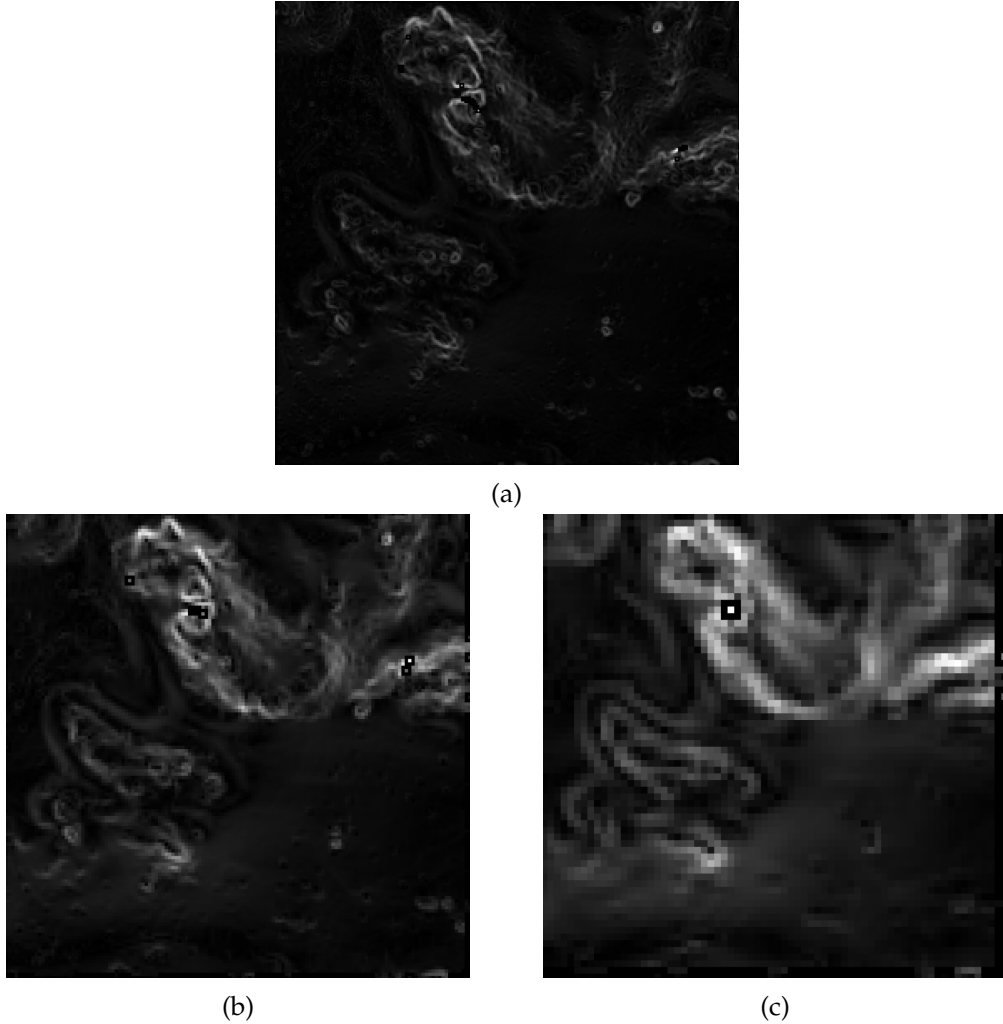


FIGURE 4.9: Comparison of global gradient map resolution. (a) Resolution of 0.5 m/pixel. (b) Resolution of 1.0 m/pixel. (c) Resolution of 2.0 m/pixel.

Although the size and resolution of the local map are parameters that we determine, they are highly limited by the on board processing power of the robot, since the higher the resolution the more computations must be performed. On the other hand, the resolution of the global map is a parameter that is determined by the equipped camera sensors of the orbiters and the reconstruction techniques applied to the imagery received from those. As the technology of the space industry advances, we

Local map resolution	Global map resolution	Matching score
0.1	0.5	97%
0.1	1.0	76%
0.1	2.0	48%
0.2	0.5	91%
0.2	1.0	67%
0.2	2.0	32%
0.5	0.5	72%
0.5	1.0	36%
0.5	2.0	25%

TABLE 4.3: Score of match for combinations of local and global map resolutions.

can expect to observe in the next few years an increase in the aforementioned resolution parameters and, consequently, an increase in efficiency of the map matching techniques. As an example, the HiRISE on board camera of the *Mars Reconnaissance Orbiter* can currently achieve a resolution of 30 cm/pixel with the possibility to acquire stereo image pairs with a precision better than 25 cm/pixel over locations of high priority, i.e. potential landing site of future missions to Mars.

Chapter 5

Conclusion

5.1 Thesis Summary

Mention briefly what was discussed in this thesis and what the experiments proved

5.2 Contributions

Mention the research and the development contribution of this thesis

- Research contributions (same as objectives of Introduction)
- Development contributions (system features):
 - Suitable for rough terrain navigation by utilizing 2.5D (elevation) maps
 - Global pose correction using map matching of local (robot-centric) and global (orbiter) elevation maps
 - Sensor-agnostic data registration using point clouds (support for lidar, stereo camera, ToF camera etc.)
 - Automatic sensor fusion when multiple inputs are provided (without prior configuration)
 - Adaptive design to fit the needs of different robots and applications

5.3 Directions for Future Extensions

Mention future work and possible extensions to the algorithm

- Use a discretized particle filter to gain advantage of the grid nature of the map
- Use global map for complete (all initial cells) or partial (new unknown cells at the map's edge) of the local map

- Use the motion model in addition to using the particle cloud distribution to determine the estimated pose's uncertainty
- Use a method (e.g. SOR) to minimize outliers in input point cloud
- Apply a threshold to points in projected point cloud that fall in the same map cell
- Implement a strategy for selecting a match in template matching when matches with similar score are a. close to each other b. far from each other

5.4 Applications

Talk about other possible applications except for the planetary one

- Autonomous driving vehicles in urban environment using a priori 3D reconstructed maps (i.e. Google Maps) - although GPS data helps in avoiding the drift of dead reckoning, global map can still be used for local map initialization
- Autonomous driving in rough non-urban areas where no predefined paths exist and GPS usage is limited
- Lunar teleoperated robot with SLAM for augmenting the operator's perception - processing is done on the station (i.e. ISS) since stereo images are sent anyway